General Disclaimer

One or more of the Following Statements may affect this Document

- This document has been reproduced from the best copy furnished by the organizational source. It is being released in the interest of making available as much information as possible.

- This document may contain data, which exceeds the sheet parameters. It was furnished in this condition by the organizational source and is the best copy available.

- This document may contain tone-on-tone or color graphs, charts and/or pictures, which have been reproduced in black and white.

- This document is paginated as submitted by the original source.

- Portions of this document are not fully legible due to the historical nature of some of the material. However, it is the best reproduction available from the original submission.

NASA CONTRACTOR REPORT 166575

APPLICATION OF LASER VELOCIMETRY TO UNSTEADY FLOWS IN LARGE SCALE HIGH SPEED TUNNELS

F. K. OWEN

CONTRACT NAS2– 11080

NASA

NASA CONTRACTOR REPORT 166575

APPLICATION OF LASER VELOCIMETRY TO UNSTEADY FLOWS IN LARGE SCALE HIGH SPEED TUNNELS

F. K. OWEN
COMPLERE, INC.
PALO ALTO, CALIFORNIA

Prepared for
Ames Research Center
under Contract NAS2-11080

National Aeronautics and
Space Administration

Ames Research Center
Moffett Field, California 94035

APPLICATION OF LASER VELOCIMETRY TO UNSTEADY FLOWS IN LARGE SCALE, HIGH SPEED TUNNELS*

by

F. K. Owen
Consultant, Complere, Inc.,
P.O. Box 1697, Palo Alto, CA 94302

*A progress report submitted in partial fulfillment of the reporting requirements of Contract NAS2-11080.

APPLICATION OF LASER VELOCIMETRY TO UNSTEADY FLOWS IN LARGE SCALE, HIGH SPEED TUNNELS.

F. K. OWEN

Complere, Inc.
P.O. Box 1697
Palo Alto, CA 94302

Abstract

Flowfield measurements obtained in several large scale, high speed facilities at NASA Ames Research Center are presented. Sampling bias and seeding problems are addressed and solutions are outlined. The laser velocimeter systems and data reduction procedures which were used in the experiments are also described. The work demonstrates the potential of the laser velocimeter for applications in other than closely controlled, small-scale laboratory situations.

Introduction

The potential of laser velocimetry for the nonintrusive measurement of mean velocity, turbulence and shear stress in complex wind-tunnel flow fields has long been recognized. However, the design, construction and successful operation of laser velocimetry systems in other than small, closely controlled laboratory situations presents a formidable engineering challenge. For time-dependent flows, considerable attention and effort has already been directed to the area of conditional sampling as a means of revealing flow features which appear intermittently rather than continuously yet still have an important influence on flow structure and development. But until recently, these efforts were all restricted to experiments in which the flow-field sensor had a continuous output which itself could be used to generate the criteria for the conditional averages; so that measurements were of necessity restricted to unidirectional shear flows in which, for example, standard hot-wire anemometry techniques could be used. Whole classes of flows, namely recirculating and unsteady wake flows have therefore been neglected.

For several years now determined efforts have been made to develop methods of predicting complex flow behaviour using numerical techniques. However, the present rate of development of computational fluid dynamics, especially for compressible flow fields, is no longer dependent on computer size or numerical techniques. Progress is currently restricted by the need for reliable test cases and an improved understanding of both the physics of turbulence and the structure of complex flows, which are required to model the turbulent correlations which result from time averaging the Navier-Stokes equations. Presently, calculation methods are unable to accurately predict compressible separated flows. This is due largely to inaccurate turbulence models applicable to turbulent separated viscous layers, a consequence of the lack of reliable experimental information. Measurements of the mean and transport properties of such flows are needed to develop improved turbulence models and to assess the accuracies of the current abundance of prediction methods.

Turbulent separated flows occur in many types of engineering configurations. They may be unintentional features of some classes of equipment or they may be deliberately introduced, but in all cases such flows can have a significant effect on overall performance. Furthermore, additional complications are added by the unsteady aspects of the turbulent boundary-layer separation and reattachment processes. Despite the fact that separated flows have been extensively studied, detailed information regarding the time-averaged, turbulent and unsteady nature of turbulent separation is practically non-existent for transonic flows. This paucity of data is not due to a lack of interest; on the contrary, the transonic Mach number range is of primary concern within commercial and military flight envelopes. The lack of data is primarily due to experimental difficulties encountered in the transonic regime.

Of particular concern in the use of total head and hot-wire probes at transonic speeds is the ever present problem of flow interference. Wake flows are extremely sensitive to local geometry with streamline curvature and associated mean static pressure gradients rendering pitot tube mean flow measurements subject to error. Problems associated with turbulent structure measurements are even more acute since linearized hotwire data interpretations are not accurate in these locally high turbulent flows. At transonic speeds the separation of the measured mode variables namely mass flux and total temperature into velocity fluctuation levels and shear stress is a complex task. As a result, hot-wire turbulence data taken in zero pressure gradient, adiabatic or isothermal attached boundary

layers show considerable scatter (Ref. 1). The differences are so great that it is impossible to construe that any form of similarity with Reynolds or Mach number exists. In flows which involve separation or time-dependent flow reversal additional problems occur which render hot-wire measurements subject to large and unknown errors (Ref. 2).

Although much more costly, laborious and tedious to operate, the laser velocimeter probably represents the instrument of last resort for the measurement of many practical flow fields. Once in operation, nonintrusive, unambiguous mean and turbulent velocities and shear stresses can be obtained once seeding and sampling bias problems have been overcome.

The purpose of the present paper is to describe the optical, seeding and data reduction procedures which have been used in the successful application of laser velocimetry to large-scale, unsteady, transonic wind-tunnel testing. The results will be illustrated with measurements of vortex flows, and ensemble-averaged data obtained for conditions of vortex-shedding, dynamic-stall airfoil oscillation, oscillating trailing-edge control flaps and helicopter rotor flow fields.

Experimental Approach

To date, measurements have been obtained during tests in the Ames 2 x 2-foot, 6 x 6-foot, 11 x 11-foot transonic wind tunnels and in the Ames Army Anechoic Hover Chamber. However, before discussing these applications the problems of sampling bias and seeding must be addressed.

The topic of laser velocimeter sampling bias has deep roots with believers and infidels debating its existence. Lack of conclusive evidence has fanned the controversy. But, most agree that continuous wave-mode signals are free from bias. However, in high-speed wind-tunnel applications where particle concentrations are low, individual realization processing is required. In these cases the potential errors attributable to sampling bias can become significant at high turbulence levels. In a recent paper (Ref. 3) the existence of "sampling bias" in individual-realization laser velocimeter measurements has been experimentally verified and shown to be independent of sample rate. The experiments were performed in a simple two-stream mixing shear flow with the standard for comparison being laser-velocimeter measurements obtained under continuous-wave conditions.

The results presented in Fig. 1 clearly demonstrate that for the individual-realization mode of laser velocimetry, sampling bias exists and that it increases approximately with the square of the turbulence intensity. It was also demonstrated that these bias effects are independent of sampling rate provided the seeding concentration is sufficiently low to ensure individual-realization measurements. A two-dimensional weighting of the velocity samples was shown to be effective in correcting the individual-realization measurements for sampling bias, Fig. 2. This correction is valid provided the length of the laser velocimeter sensing volume is reasonable long in comparison to its cross section. (This is generally true for most laser-velocimeter systems). Although a confirmation of sampling-bias effects on higher-order turbulence quantities, such as the turbulence intensities and Reynolds shearstress, could not be made since there is no standard at high turbulence level, the results suggest that the statistical estimators for these quantities must also include appropriate weighting for sampling bias.

Maximum optical system sensitivity is also essential for meaningful measurements particularly in large wind tunnels. In these applications solid angle light collection is reduced so that there is always the possibility that only the velocities of larger particles, which may not follow the flow, will be observed. This could result in errors in the mean flow and turbulence measurements and difficulty in obtaining data in vortex cores. Previous measurements have stressed the value of forward scatter optical systems whenever possible, since data rates which are orders of magnitude higher than those in the back scatter mode can be achieved. Rather than relying entirely on natural wind-tunnel aerosols for the light scattering, it is advisable to introduce an artificial aerosol of known size distribution which can be generated with an ultrasonic nozzle mounted in the wind tunnel downstream of the test section. The size distribution of such an aerosol with a count mean diameter of less than one micron is shown in Fig. 3. Such aerosols have been found adequate for turbulence studies of shock boundary-layer interactions and vortex flows at transonic and supersonic speeds. To confirm this, axial and vertical velocity measurements have been obtained at variable threshhold settings on the processing electronics. At high settings, only a few of the larger particles which passed through the center of the probe volume were considered, whereas at low threshhold settings velocities of the submicron particles dominated. Even in vortex cores the mean flow angle varied less than 3° with threshhold setting changes which reduced the velocity data rate from 16,000/sec to 1,000/sec. These results were in substantial agreement with data obtained with natural seeding. So that, in general, seed material need only be introduced when high data rates necessary for conditional sampling or spectra measurements are required.

The Ames Laser Velocimeter Systems

2 x 2-Foot TWT

Velocity measurements were made with the laser velocimeter shown schematically in Fig. 4. This system was designed and built by NASA for the Ames 2 x 2-Foot transonic wind tunnel. This fringe-mode velocimeter is a dual-color system utilizing the 4880 and 5145 Angstrom lines of an argon-ion laser. One spectral line is used to measure the streamwise velocity component, the other to measure the vertical velocity component. Bragg-cell frequency shifting necessary for probing highly turbulent and separated flow regions is incorporated in both spectral lines. The frequency offsets also facilitate the direct measurement of the vertical velocity compo-

nent (i.e., ±45° beam orientations to resolve the vertical velocity are unnecessary). As seen in Fig. 4 most of the optical components are located outside the tunnel plenum chamber, where color separation, Bragg-cell frequency shifting, and the establishment of the four-beam matrix are accomplished. Only the transmitting optics, collecting lens, and photo detectors are mounted inside the plenum chamber. The one on the opposite side of the test section from the laser holds the collecting lens and photo detectors for forward-scatter light collection. The traversing system on the laser side of the test section supports the transmitting lenses. Mirrors fixed to this traversing system permit three-dimensional scanning of the velocimeter's sensing volume; the optics outside the plenum chamber remain stationary. Both traversing systems are driven with computer-controlled stepper motors. The effective sensing volume is approximately elliptic, 200 μ in diameter and 3mm long, with the axis aligned in the cross-stream direction. Signal processing is accomplished with single-particle burst counters. The individual realizations from the two channels and arrival time are simultaneously recorded.

Naturally occurring particles in the tunnel are normally used for light scattering. In this facility, lubrication oil within the drive system vaporizes and then condenses in the tunnel circuit to provide a generous supply of scattering centers. Previous measurements across a normal shock have shown that these particles are small enough in size (estimated to be 1 μ) to give very good response to a step change in velocity at sonic speeds. At each point in the flow, several thousand velocity realizations are generally used to calculate the flow properties.

6x6-Foot TWT

In more recent work the capabilities of a new dual beam forward scatter LDV system for the Ames 6x6-foot wind tunnel have been demonstrated. A photograph and schematic of this laser velocimeter is shown in Fig 5. With this system the velocity field in the wake of a body at points in the cross-flow plane (perpendicular to the model) can be measured with this two-color, forward scatter, frequency offset system which enables the simultaneous measurement of two independent velocity components. Again, two primary laser lines, namely 4880 and 5145 A, are separated by means of a prism, P. These primary beams are each split by Bragg cells B_1 and B_2 to obtain two pairs of divergent, frequency-offset beams. Each pair of beams is then passed through cubes (C_1 and C_2) which are ground to be slightly "off-square" to rectify the divergence. The four resultant parallel beams proceed through the sending optics and are focused at the same point within the flow test region. Collecting optics on the far side of the wind-tunnel test section refocus the scattered light onto a pair of photomultiplier tubes. The signals from those tubes are then processed to obtain two components of velocity of particles passing through the focal volume. The sensing volume determined by beam crossover volume, off-axis collection and spatial filter size resulted in an elliptic sampling volume with principal axes of 0.1 mm (diameter) and 1 mm (spanwise) respectively. Measurements have been made within 1 mm of the surface during wind-tunnel testing. The Bragg cells, which produce zero-velocity frequency offsets in both color systems, were incorporated to remove directional ambiguity.

Modifications can also be made to the 6x6-foot wind tunnel optics. This change enables either the 4880 or the 5145° lines to be passed through a plane-cylindrical lens system so that a sheet of laser light can be generated to illuminate water vapor in the cross flow plane, thus providing vapor-screen visualization of the flow field (see Fig. 6). By changing the location of the beam focus, a sheet of variable thickness and divergence angle can be produced. The lens can be rotated manually about the y-axis and longitudinally and vertically using the velocimeter traverse gear such that any cross-sectional plane in the flow within the field of view circumscribed by the tunnel window can be observed. This traversing flexibility, accuracy and focused light sheet has enabled superior vortex flow visualization compared to that with previous mercury vapor light sources. Water is introduced into the flow and a thin cross-section, about 2 mm thick is illuminated. Such a thin sheet enables detailed visualization of vortex cores, feeding sheets and flow-field structures. Photographs are taken with a camera mounted on the sting/strut support.

11x11-Foot TWT

A schematic of the beam system used in a recent oscillating flap test is shown in Fig. 7. As with the 2x2-Foot TWT system, the laser and most of the optics are located outside the tunnel where a two-component beam matrix is established. Scanning and receiving optics are mounted in the tunnel plenum chamber.

Ames Army Anechoic Hover Chamber

The system used recently in a helicopter blade rotor study is shown in Fig. 8. It was designed and built to measure all three components of induced perturbation velocities by freezing the flow at two different azimuthal positions. Ensembled averages of the time-dependent flow in the tip region were obtained using a one/rev. pulse originating from the drive assembly. Measurements have been made using a 3.0 inch chord NACA 0012 untwisted, untapered airfoil with a rotor radius of 41 inches. At nominally zero angle of attack, data were obtained for tip Mach numbers. of 0.85, 0.88, 0.9 and 0.95 in a minimum of three inboard and outboard planes with emphasis on the region of maximum shock strength and at the location of the sonic cylinder. At 8° collective pitch and a Mach number of 0.4, measurements were made of the trailing vortices by a straightforward adjustment of the data window.

Data Reduction

To support the work, a three-dimensional data acquisition and reduction program was written for the HP9845 desk-top computer. This program enables

either 1, 2 or 3 components of laser velocimenter data to be processed. Up to 2,500 readings from a multiplexer, LDV/computer interface, can be accepted at one time. Each reading contains the information required to calculate the instantaneous velocities u, v, w. From these determinations, the average velocities $\bar{u}$, $\bar{v}$, $\bar{w}$, turbulence levels u', v', w' and the cross correlations $\overline{u'v'}$, $\overline{v'w'}$, $\overline{u'w'}$ are all calculated. Plots of these parameters are displayed on line as profiles are measured and hard copy is available as required. All the raw and reduced data are stored on flexible discs for permanent storage and retrieval. Real time histograms, probability densities of all three velocity components are displayed during data acquisition.

A two-dimensional unsteady flow program was also written for the HP 9845 desk-top computer. In this case, readings from the multiplexer contain information to calculate two instantaneous velocity components and time of arrival. From these determinations ensemble averages, throughout the unsteady period, can be generated. For each "data window", which can be varied, $\bar{u}$, $\bar{v}$, u', v' and $\overline{u'v'}$ are calculated and displayed on line along with the histograms. At the conclusion of each profile plots can be generated. Once again all the raw and reduced data are permanently stored on flexible discs.

Flow-Field Measurements

Vortex Measurements

Tests have been conducted in the Ames 2-x2 ft. Transonic Wind Tunnel at a freestream Mach number of 0.6 and unit Reynolds number of 2 million/ft. Wake vortex measurements were obtained for a 1-in. diameter tangent ogive which had a nose fineness ratio of 3.5 and a total or body fineness ratio of 12:1. Flow-field measurements were obtained at two axial stations at angle of attack of 36 deg. (Ref. 4). Measurements have also been made, in the 6 by 6-Foot TWT, of the wake of a 3-inch diameter circular cylinder with a two-caliber tangent ogive nose. The total length to diameter ratio was 15. Wake measurements were made at a number of axial stations and angles of attack at a Mach number of 0.6 and Reynolds number based on body diameter of 0.62 million. These results represent the first LDV measurements of a compressible body vortex wake at high Reynolds number. Fig. 9 shows the cross-flow velocity measured in a plane eight diameters from the nose at moderate incidence. This case of nearly symmetric vortex flow, shown schematically in the figure, reveals significant overshoots close to the body, high mean gradients which occur across the feeding sheets, and a large deficit in the wake. These wake deficits and mean gradients measured close to the body are both much larger than those measured previously at low speeds. However, both these features decay quite rapidly, an indication of energetic turbulent motions in the wake. The profiles have the form expected of two symmetric-free vortices except near the wake centerline where vortex interaction appears to dominate.

The profiles for $M_\infty = 0.6$, $\alpha = 45$ deg, and $x/d = 8$ are shown in Fig. 10. For this angle of attack the lateral shift in vortex locations is evident. The y/d position of the minimum value of $\bar{w}$ moves from - 0.267 at $z/d = 1.167$ to 0.433 at $z/d = 3.167$. Comparing this to the appropriate vapor-screen photograph (shown schematically), it is seen that this is consistent with the portside displacement of the vortex nearest the body and the starboard displacement of the subsequent vortex.

Some insight into the turbulent and unsteady nature fo the vortex flow field has also been obtained from the laser velocimeter measurements. Consider first the mean and rms axial velocity profiles across the wake at $x/d = 6$. These data (Fig. 11), obtained at $z/d = 0.9$ for a symmetric flow case clearly show double peaks in the rms velocity, one on each side of the wake centerline close to the regions of maximum mean velocity gradient. However, there are also significant rms fluctuation levels in regions of small and zero mean velocity gradient, indicating that larger scale turbulent or unsteady motions are present. Indeed, in the region of the time-averaged velocity zeros ($y/d = \pm 0.4$), bimodal velocity probability density distributions were observed. But insight into the relative contributions of the large-and small-scale motions can only be determined by ensemble averaging.

Time-Dependent Measurements

Unfortunately, laser velocimeter data alone are usually difficult to conditionally sample since in most cases the data rates are insufficient to generate real-time information from which the sampling criteria can be determined. A technique close to conditional sampling can be used to generate ensemble averages at given phase angles in turbulent flows superimposed on periodic motions, such as those in reciprocating machinery or helicopter wakes, for example. In these cases, the sampling condition can be derived from a periodic timing signal. However, in the case of aerodynamic oscillations, whose period is not exactly constant, for example, the flow behind a bluff body. The sampling condition should be derived from the flow itself.

In Ref. 5 a combined nonintrusive surface thin film gage and laser velocimeter technique was described which can be used to obtain new information on the phase averaged and turbulent structure of time-dependent flow fields. These experiments were conducted in the Ames 2x2-Foot wind tunnel on a circular cylinder of aspect ratio 24:1 in crossflow over a range of Reynolds numbers in the subsonic and transonic regime. The cylinder was instrumented with constant temperature surface hot film gages. The dynamic gage response (greater than 60 kHz with negligible phase distortion) was sufficient to determine the time history of the vortex shedding. The gage outputs were used to trigger a forward scatter laser velocimeter which generated conditionally sampled axial and vertical velocity distributions in the unsteady vortex flow behind the cylinder. Detailed information obtained by this sampling technique on the time-dependent

mean flow field behind a circular cylinder and of the large- and small-scale turbulent structure of its wake were presented.

To illustrate some of these measurements, data taken in the wake 2.5 diameters downstream of the cylinder (x/d = 2.5) are shown in Fig. 12. On the wake centerline, positive and negative vertical velocities are equally probable. Thus, conventional averaging would give a time-averaged velocity close to zero and a large rms velocity fluctuation level which is, of course, due to instantaneous changes in induced mean flow velocity caused by alternate vortex shedding. Any time-dependent information would be lost. Above the centerline (y/d = 0.5), the probability density function is still bimodal, although negative vertical velocities predominate, as here the local flow is determined more by vortex shedding from the upper surface. In this case, conventional averaging would indicate a small negative vertical velocity, a large rms and, once again, time-dependent information would be lost. Below the axis (y/d = -0.5), positive vertical velocities induced by vortex shedding from the lower surface are more likely, but again, conventional averaging would lose the true nature of the timedependent local flow field. Outside the wake (e.g., y/d = -1.75), where single-peaked probability distributions occur, time-averaged data interpretation is sufficient.

To determine the time-dependent nature of the wake, the bimodal velocity distributions must be conditionally sampled using the thin-film gage output. Since the flow repeats itself periodically, we can sample the velocity when the shedding vortices are at some given position in the flow as determined by the time-dependent thin film gauge voltage signature. One cycle later we can sample again, and thus, over many cycles, build up an ensemble average at constant phase. These velocities represent the regular- and small-scale random behavior of the flow at a fixed point in the flow field with the vortices frozen in some average position. Data obtained throughout the shedding cycle are shown in Fig. 13 where it can be seen that the conditionally sampled vertical velocity variations are approximately sinusoidal, their period corresponding to that of the Strouhal shedding frequency.

Fig. 14 shows a comparison of the axial and vertical rms velocity fluctuation levels measured across the wake at x/d = 2.5. As mentioned previously, the apparent vertical velocity fluctuations are extremely high in the center of the wake. However, when phase-sampled, the small-scale turbulence data fall below the axial centerline turbulence measurements. Assuming isotropic small-scale turbulence in the wake, we can infer that there is a vortex-induced contribution to the axial turbulence on the wake centerline. The large differences in the rms vertical velocity data also show the dominance of the large-scale structures in the vertical wake turbulence. It is clearly incorrect to attempt to model these large rms fluctuation levels with techniques that are only valid for small-scale turbulence. In general, it is equally insufficient to attempt to use current turbulence models scaled to match rms velocities measured in the conventional manner in any flow where unsteady phenomena are likely to be encountered, separated flows being a prime example.

Conditionally sampled, simultaneous two-component laser-velocimeter measurements have also been obtained for the case of an oscillating airfoil at M = 0.4 at reduced frequencies ($\omega c/u$) of .12 and 1.2, in the Ames 2x2-foot wind tunnel. A schematic of the measurement procedure is shown in Fig. 15 where signal processing is accomplished with single particle burst counters. In the system, a once-per-revolution pulse originated by the airfoil drive mechanism resets the multiplexer clock so that clock pulse number represents the instantaneous airfoil angle of attack throughout each cycle. Now, as particle arrival times are random the clock pulse number can be used to assign each velocity measurement to its correct phase ensemble. The two velocity components (u, v) and clock pulse number are recorded on floppy disc for analysis. Reynolds stress measurements were also obtained by requiring coincidence of the two velocity components before each data set was accepted. Software developed specifically for this test program enabled probability densities of each velocity component and velocity cross products to be determined on line for selected angle-of-attack "windows". From this information, ensemble averages of $\overline{u}$, $\overline{v}$, $\overline{u'}$, $\overline{v'}$ and $\overline{u'v'}$ were calculated. Phase averaged mean velocities and turbulence quantities were measured at two streamwise locations; namely, x/c = 0.45 and 1.06, i.e., at approximately mid-chord and in the near wake. Profiles were obtained at oscillation frequencies of 2.8 and 28 Hz.

Emsemble-averaged axial velocity profiles are shown in Figs. 16 and 17. The most obvious feature of these results is the large hysteresis which exists as the airfoil oscillates in and out of stall. This hysteresis is even more pronounced at the higher frequency. In both cases, at x/c = .45, the flow is attached at ten degrees when the angle of attack is increasing. Both flows are clearly stalled at 15 degrees with the 28 Hz case being more extensive. When the airfoil returns through 10 degrees, recovery appears more complete for the 2.8 Hz case. In the near wake (x/c = - 1.06) these differences are accentuated and the effect of frequency more pronounced. At ten degrees increasing angle of attack the low frequency profile shows a wider wake with a greater velocity deficit an indication of earlier dynamic stall. At fifteen degrees, however, the higher frequency wake profile shows that much more extensive flow separation has occurred on the airfoil consistent with the x/c = .45 profiles. This indicates a significant loss of lift compared to the 2.8 Hz case. The profiles obtained as the airfoil retreats through 10 degrees clearly show the greater hysteresis in the 28 Hz case. Thus the essential flow-field features revealed by these profiles tells us that angle-of-attack oscillations through the static stall value produce significant flow-field hysteresis. Increasing the reduced frequency of oscillation delays the onset of dynamic stall but recovery is also delayed. This must result in a large C_L vs α hysteresis loop.

Measured axial velocity fluctuation levels presented in Figs. 16 and 17 are consistent with the mean profile observations. In the near wake at 10 degrees, increasing angle of attack the RMS velocity fluctuations are significantly higher in the 2.8 Hz case again an indication of earlier onset of dynamic stall. At 15 degrees the 28 Hz case shows higher turbulence levels even though the mean gradients in the wider wake are less, indicating large-scale turbulent mixing. Delayed stall recovery at 28 Hz is again evident at 10 degrees decreasing angle of attack since there is still evidence of much more extensive large-scale turbulence in the wake. Data taken on the airfoil confirms these trends.

Although these ensemble mean and RMS velocity profiles give us a good deal of insight into this particular study of dynamic stall, further measurements are needed for us to assess turbulence models currently employed in prediction methods. The instantaneous velocity at a point in the flow field may be expressed as

$$u = \bar{u} + \overline{u}' + \tilde{u}$$

where $\bar{u}$ is the conventional mean, u' is the random fluctuation and u is the unsteady contribution from the oscillating angle of attack. This term will vary in both amplitude and phase as a function of instantaneous angle of attack and reduced frequency. With a similar expression for the vertical velocity and insertion in the momentum equation we obtain

$$\bar{u}\frac{\partial \bar{u}}{\partial x} + \bar{v}\frac{\partial \bar{u}}{\partial y} = -\frac{1}{\rho}\frac{\partial \bar{p}}{\partial x} + \nu\frac{\partial^2 \bar{u}}{\partial y^2} - \frac{1}{\rho}\frac{\partial}{\partial y}\left[\overline{u'v'} + \overline{\tilde{u}\tilde{v}}\right]$$

if we assume that the random and time-dependent scales are uncorrelated.

The major assumption in all current unsteady calculations is that the phase-averaged Reynolds stress distribution is related to the phase-averaged velocity profile as in the steady case

$$\langle u'v' \rangle = \varepsilon \frac{\partial \langle u \rangle}{\partial y} \quad , \quad \varepsilon = \ell^2 \left|\frac{\partial \langle u \rangle}{\partial y}\right|$$

We can see that this assumption is valid only if $\overline{u'v'}$ is unaffected by the oscillation and $\overline{u'v'} >> \overline{\tilde{u}\tilde{v}}$.

A first attempt to determine the validity of these assumptions has been made by measuring the ensemble-averaged Reynolds shear stresses in the near-wake region. The results for the case of 2.8 Hz are presented in Fig. 18. These averaged profiles show extremely high shear stress values in the dynamically stalled cases. Indeed, mixing length estimates obtained from these measured values and the slopes of the ensemble-averaged mean velocities indicate mixing lengths 4 to 5 times greater than those for steady stall cases. This challenges the validity of the quasi-steady calculation procedures since it appears that the characteristic vortex shedding feature of dynamic stall leads to mixing lengths significantly larger than those observed in the steady stall case.

These results confirm the need for ensemble-averaged measurements of complex unsteady turbulent flow fields. Ensemble-averaged mean profiles should provide challenging test cases for computation and the turbulence and shear stress information should foster the development of appropriate turbulence closure models. These early results challenge the basic quasi-steady assumptions currently employed in computational schemes. Consequently the measurement and prediction of these flows will present a formidable challenge for many years to come.

Time-dependent measurements have also been made recently in a much larger transonic facility, namely the Ames 11 by 11-Foot TWT. During this test, a 29-inch chord, 54-inch span NACA 64A010 airfoil was held between two splitter plates. The airfoil consisted of a fixed front and a trailing edge flap of 25% chord which could be oscillated up to 60 Hz at amplitudes to ±6 degrees. Data were obtained for fixed airfoil angles of attack of zero and 4 degrees at pressures of 0.5 and 2.0 atmospheres and at a freestream Mach number of 0.85.

Static measurements shown in Fig. 19 show the symmetry of the near-wake at zero angles of attack where there is excellent similarity between the laser velocimeter and pitot wake profiles, although true axial veolicity cannot be determined from pitot profiles without static pressure gradient assumptions. However, at 4 degrees (Fig. 20)there are marked differences, the pitot probe indicating incipient separation probably due to probe interference, whereas the velocimeter profiles show only a thick retarded upper layer with significant entrainment and a thinner attached lower boundary layer, consistent with measured surface pressure distributions.

Ensemble-averaged measurements for the case of 30 Hz flap oscillation are shown in Figs. 21 for zero fixed airfoil angle of attack and a mean flap position of 4 degrees. This sequence shows that at 2 degrees flap angle the upper surface flow is again retarded by the adverse pressure gradient, at 4 degrees the wake deficit and width are increased and at 6 degrees significant wake displacement can also be seen in addition to still greater wake effects. A comparison of the measured vertical velocities shows increased wake deflection angles with increasing flap deflection. These results obtained with transmitting and receiving optics separated by fourteen glass surfaces (i.e., seven sheets of glass) clearly confirm the potential of LDV for large-scale, high-speed testing.

Finally, predictions of acoustic waveforms are known to be dependent upon accurate knowledge of the near-field perturbation velocities in the tip region of helicopter rotors. With this in mind, laser velocimeter measurements of rotor flow fields have recently been completed in the Ames Army Anechoic Hover Chamber. The present results represent the first three component measurements of the near-field perturbation velocities of a model helicopter in hover and, as such, should provide valuable input and comparisons to current small disturbance codes. The data will also provide for direct comparisons to more limited hot-wire measuremenets and for the calculation of

chordwise pressure distributions to compare with 3D flow-field calculations.

To illustrate some of these results, the nature of the induced chordwise perturbation velocity profiles in the tip region are shown in Fig. 22. These data, obtained for a tip Mach number of 0.95 show that a strong shock exists inboard of the tip and is swept chordwise over the outer portions of the blade extending beyond the tip.

Tangential and radial velocity measurements have also been made. These data can provide insight into the structure of the trailing vortices. Fig. 23, shows an example obtained at a tip Mach number of 0.4 and 8 degrees collective pitch. It can be clearly seen that the trailing vortex has an outer "free" vortex form (i.e., $V \alpha 1/R$) with an inner viscous core. Here rotation is essentially solid-body (i.e., $V \alpha R$) and the circulation varies as the square of the distance from the vortex center. Within the viscous core seed particle accelerations are substantial. For the case shown in Fig. 23, accelerations of 2000g (in the Eulerian frame) occur across the core. Although this puts a severe test on the seed particles, no "black holes" were apparent during the test. It is felt that these results demonstrate the strong potential of the laser velocimeter for the ensemble-averaged measurement of rotor flow fields and the ability of the technique to freeze the flow over many revolutions to track trailing vortices.

Concluding Remarks

Conventional and ensemble-averaged laser velocimeter measurements have been accomplished for a variety of test conditions in a number of large-scale, high-speed facilities at NASA Ames Research Center. These measurements demonstrate the potential of the laser velocimeter for applications in other than closely controlled, small-scale laboratory situations. However, before extensive large-scale research programs are undertaken in major wind tunnels, attention must be directed to remote alignment capability. This will enable longer run times and more efficient tunnel operation.

Acknowledgement

The author wishes to express his thanks to the Ames Research Center of NASA for support under Contract NAS2-11080.

References

1. Fernholz, H. H. and Finley, P. J., "A Further Compliation for Compressible Boundary Layer Data with a Survey of Turbulence Data," AGARD-AG-263, Nov. 1981.

2. Owen, F. K., "An Assessment of Flow-Field Simulation and Measurement," AIAA Fluid and Plasma Dynamics Conference, July 1983.

3. Johnson, D. A., Modarress, D. and Owen, F. K., "An Experimental Verification of Laser-Velocimeter Sampling Bias and Its Correction," In Engineering Applications of Laser Velocimetry, ASME Winter Meeting, Nov. 1983.

4. Owen, F. K. and Johnson, D. A., "Wake Vortex Measurements of an Ogive Cylinder," AIAA J. Aircraft, Vol. 16, No. 9, Sept. 1979.

5. Owen, F. K. and Johnson, D. J., "Measurement of Unsteady Vortex Flow Fiels," AIAA Journal, Vol. 18, No. 19, 1980.

Figures

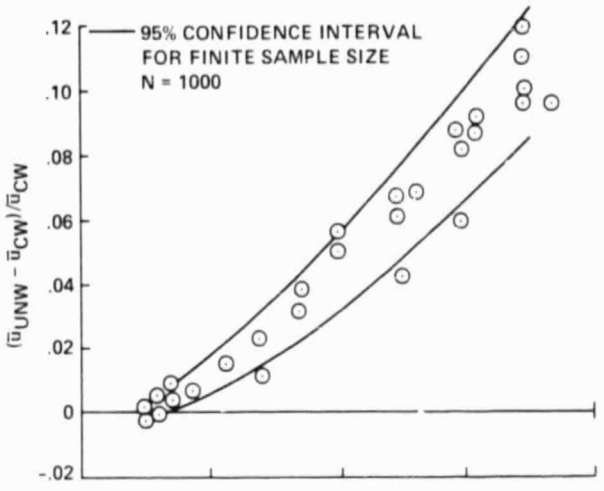

Fig. 1. Measurement error due to sampling bias (Ref. 3)

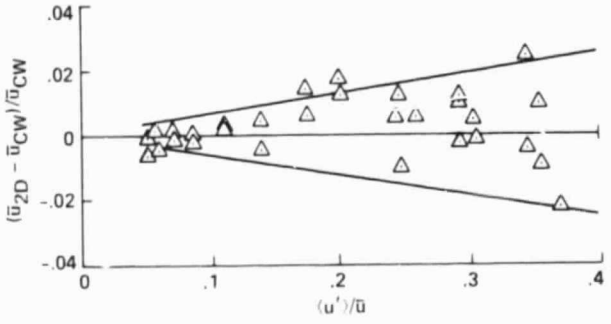

Fig. 2. An assessment of 2D weighted correction for sampling bias (Ref. 3)

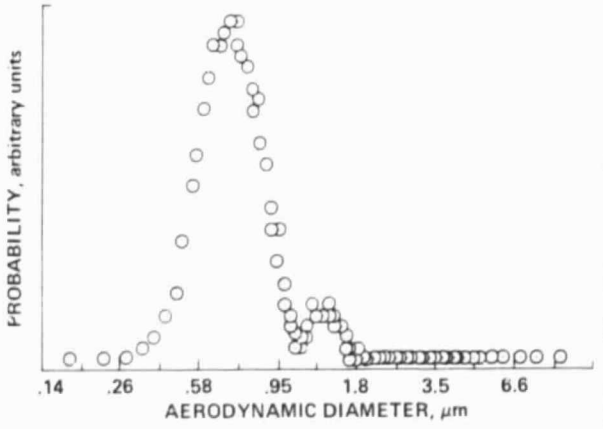

Fig. 3. Seed particle size distribution

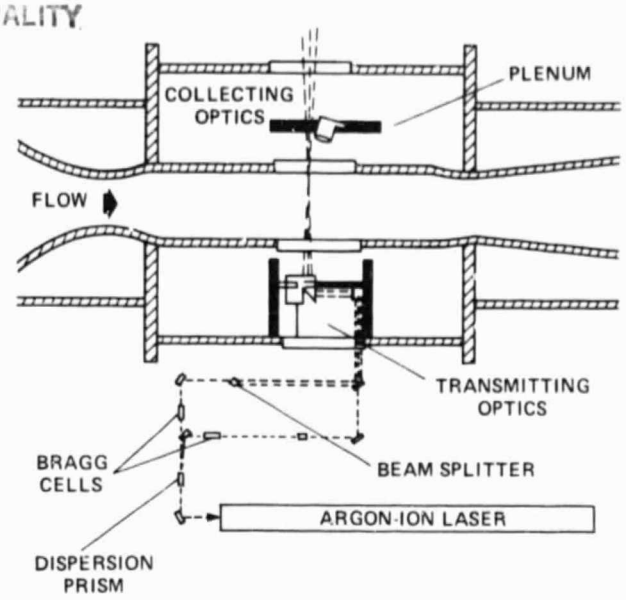

Fig. 4. Laser velocimeter for Ames 2-foot Transonic wind tunnel

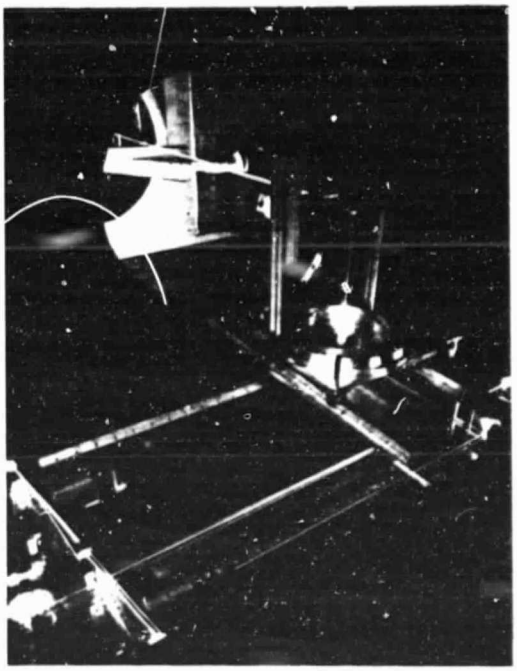

Fig. 5a. Photograph of the Ames 6-foot laser velocimeter system

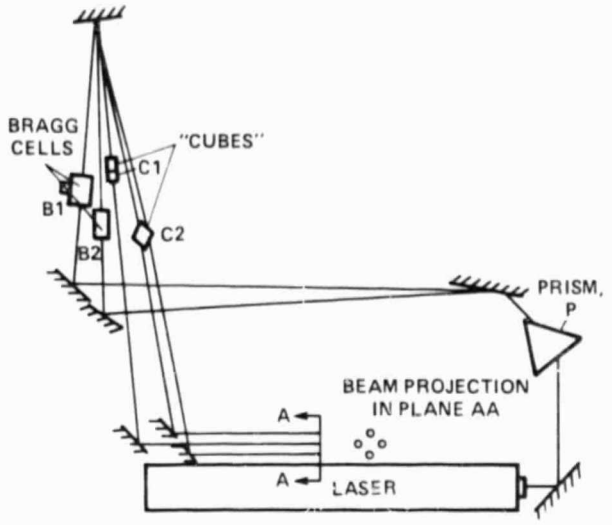

Fig. 5b. Schematic of the Ames 6-foot laser velocimeter system

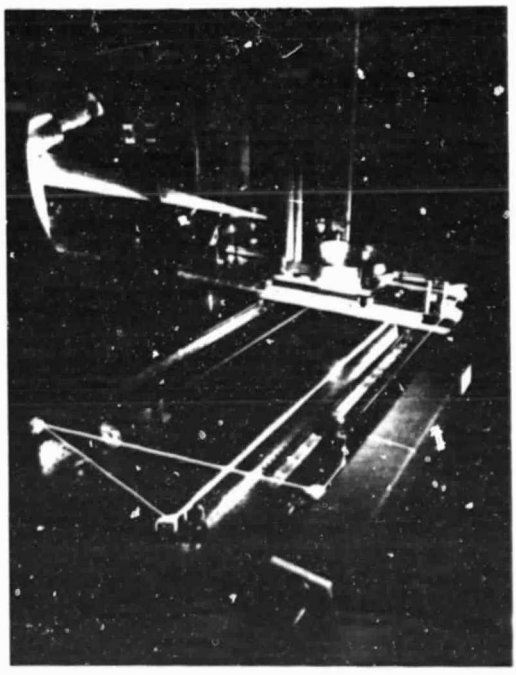

Fig. 6. Laser vapor screen--Ames 6-foot tunnel

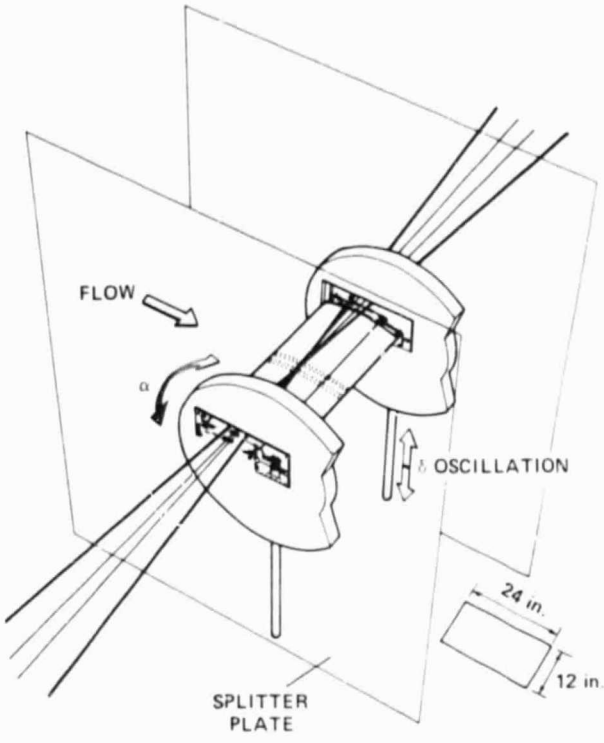

Fig. 7. Beam system for Ames 11-foot tunnel

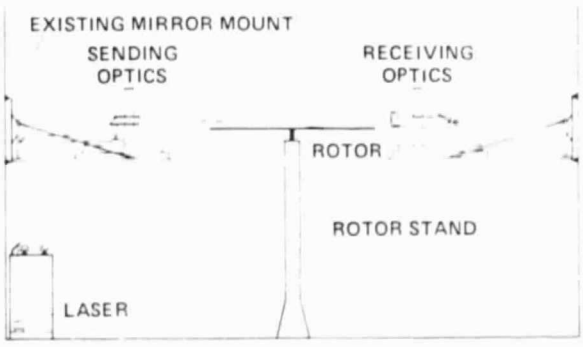

Fig. 8. Laser system for Ames-Army anechoic chamber

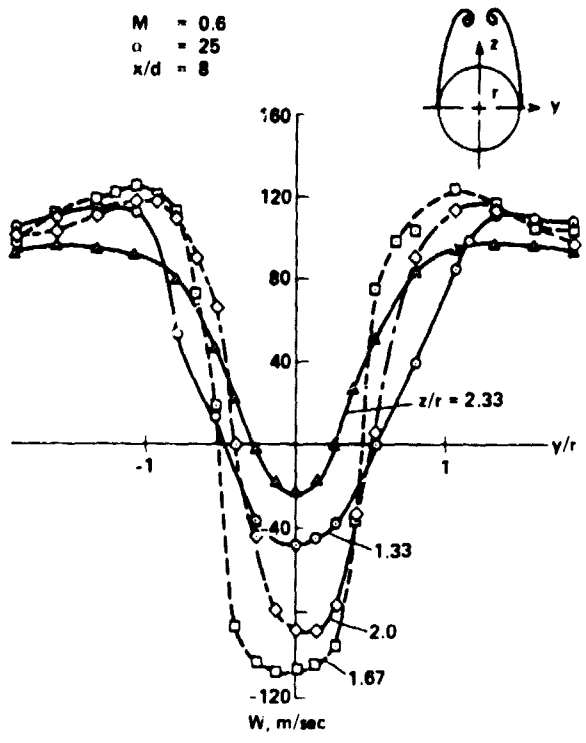

Fig. 9. Symmetric wake vortex measurements, Ames 6-foot tunnel

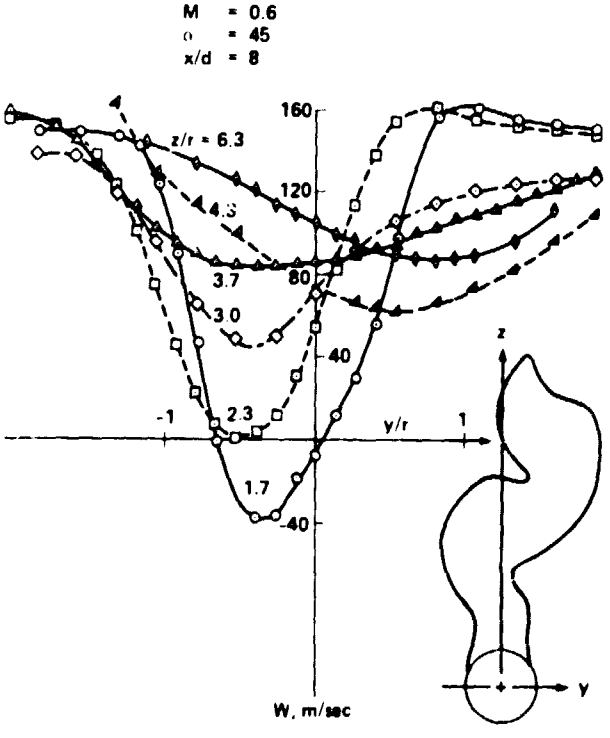

Fig. 10. Asymmetric wake vortex measurements, Ames 6-foot tunnel

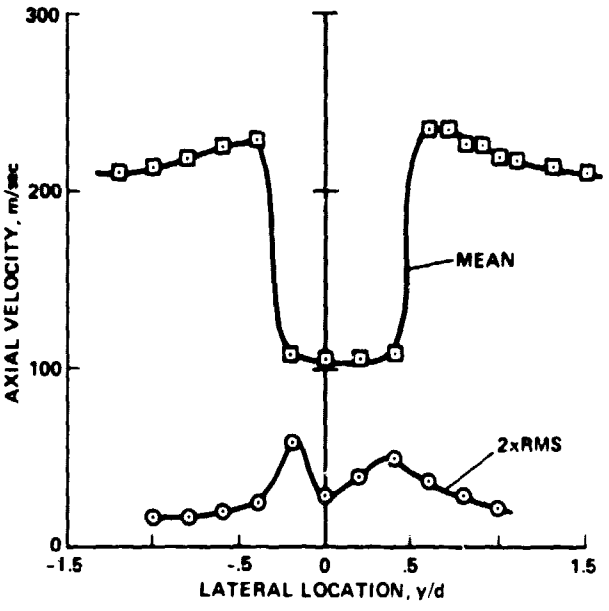

Fig. 11. Mean and RMS velocity profiles across a wake vortex

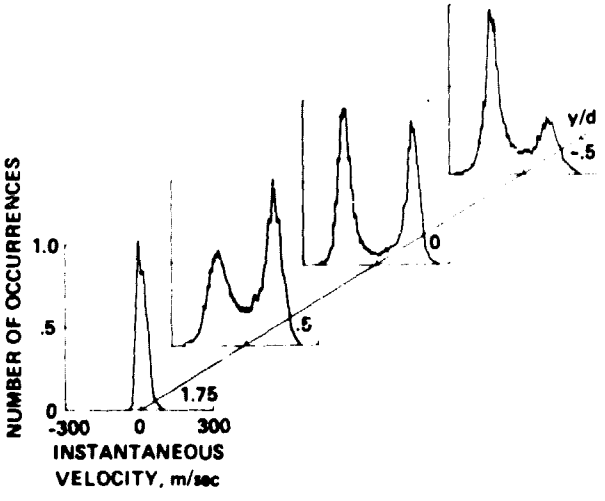

Fig. 12. Velocity probability density measurements across a cylinder wake

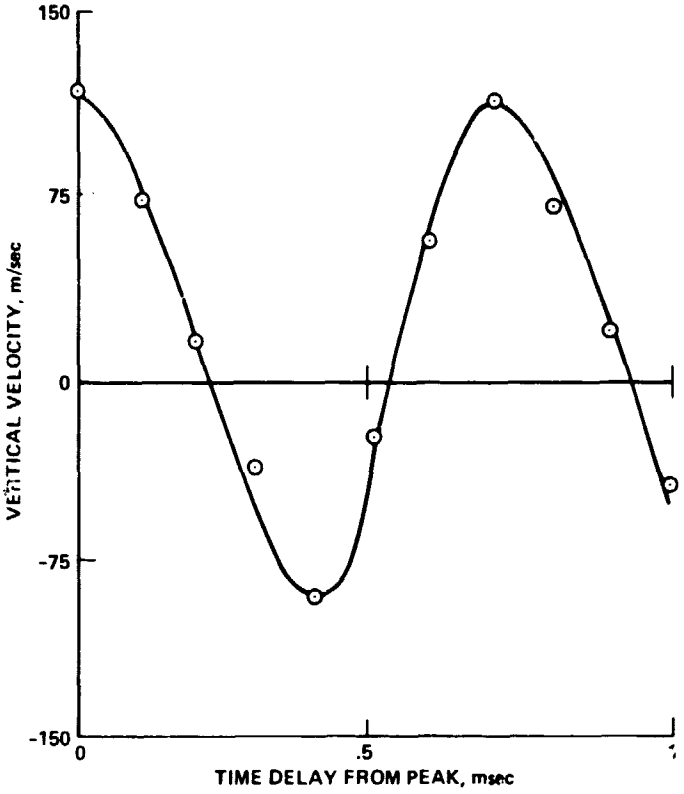

Fig. 13. Conditionally sampled vertical velocity variations in a cylinder wake

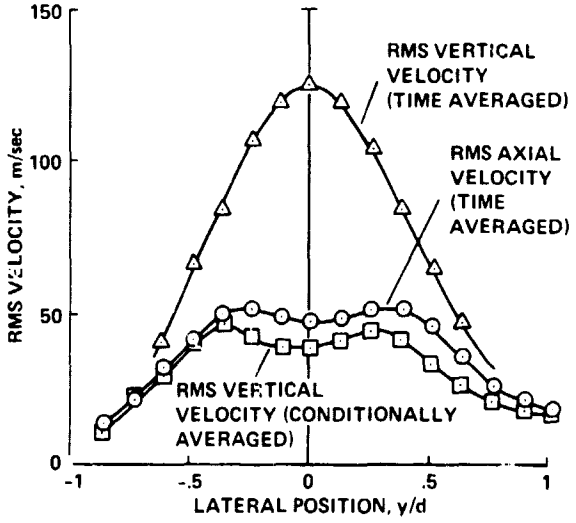

Fig. 14. Root mean square velocity profiles across a cylinder wake

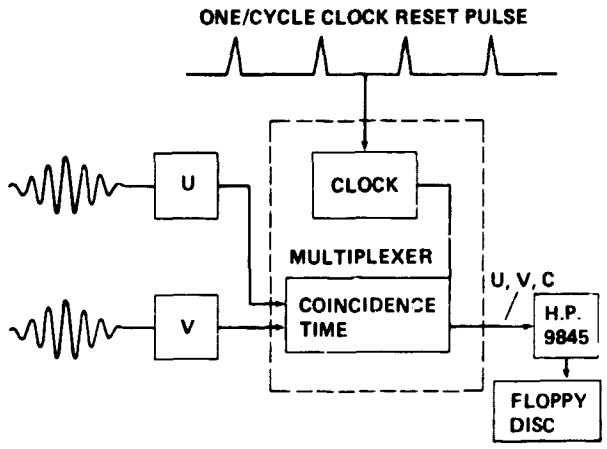

Fig. 15. Schematic of a conditional sampling data system

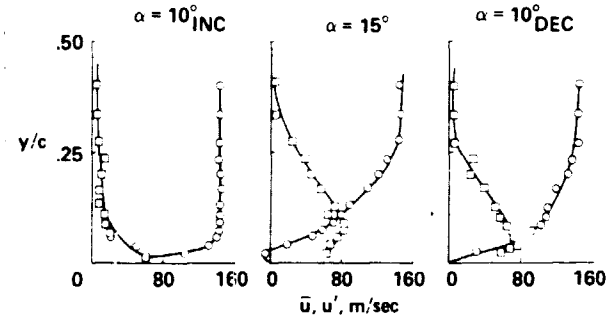

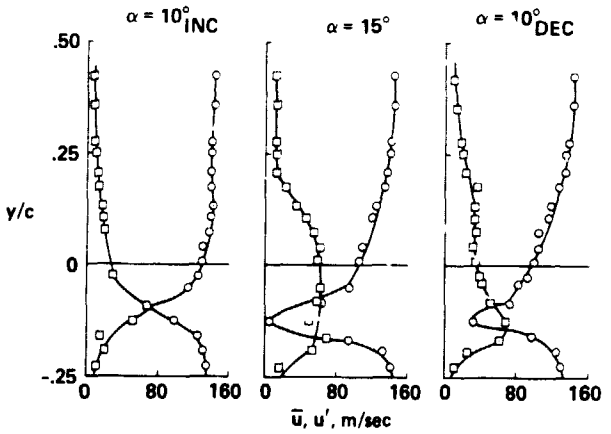

Fig. 16. Ensemble averaged streamwise mean and turbulent velocity profiles obtained on an oscillating airfoil at a reduced frequency of 0.12. a) x/c = 0.45, b) x/c = 1.06.

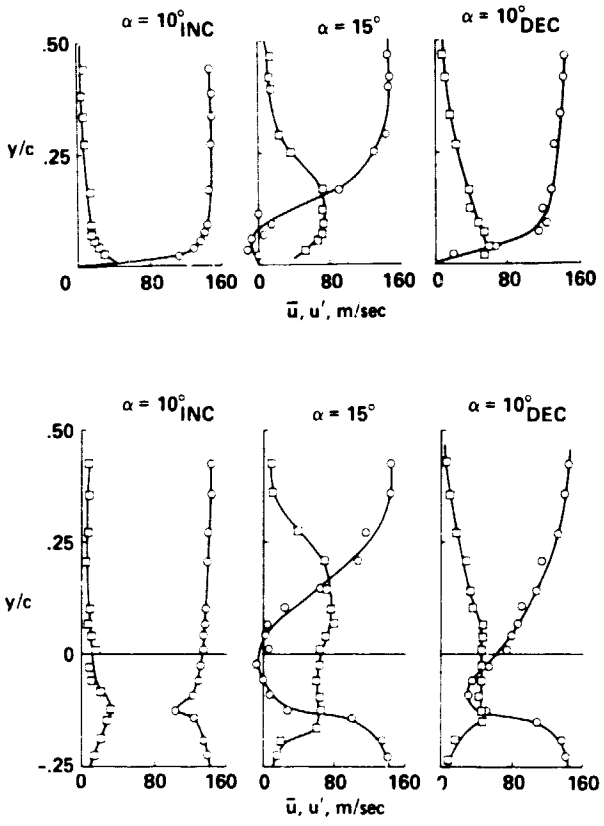

Fig. 17. Ensemble averaged streamwise mean and turbulent velocity profiles obtained on an oscillating airfoil at a reduced frequency of 1.2. a) x/c = 0.45, b) x/c = 1.06

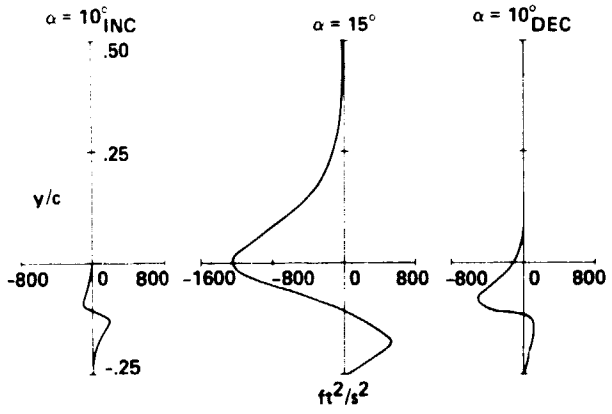

Fig. 18. Ensemble-averaged Reynolds shear stress distributions for a reduced frequency of 0.12.

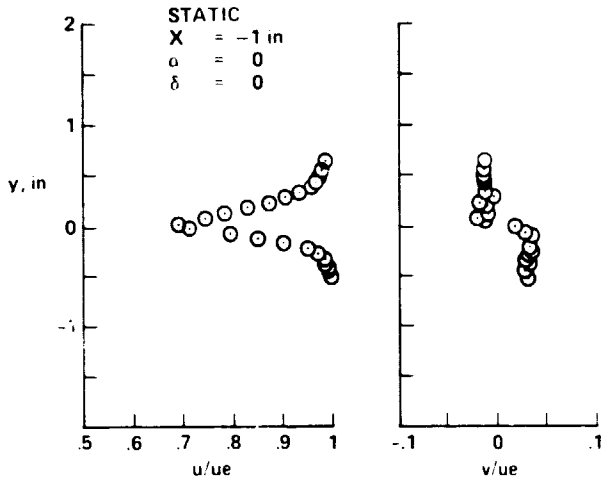

Fig. 19. Static wake profile measurements, Ames 11-foot tunnel

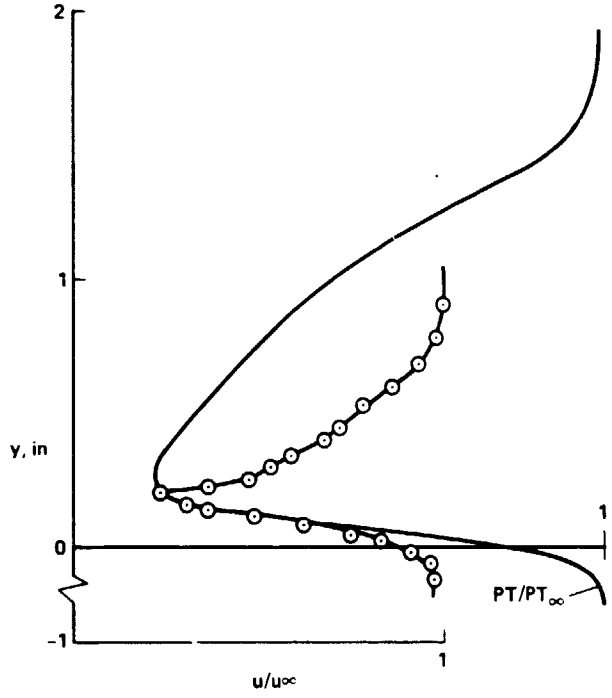

Fig. 20. Comparison of laser and pitot measurements, Ames 11-foot tunnel

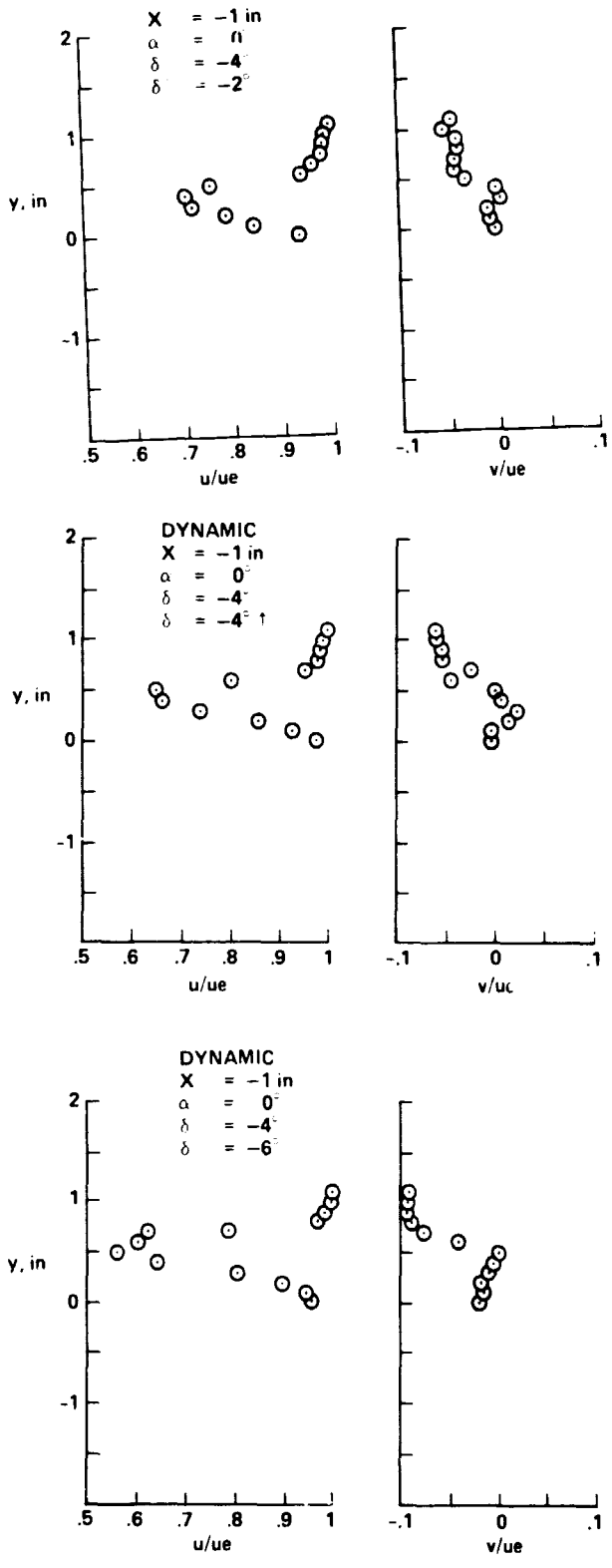

Fig. 21. Ensemble averaged measurements for the case of 30 Hz flap oscillation, Ames 11-foot tunnel

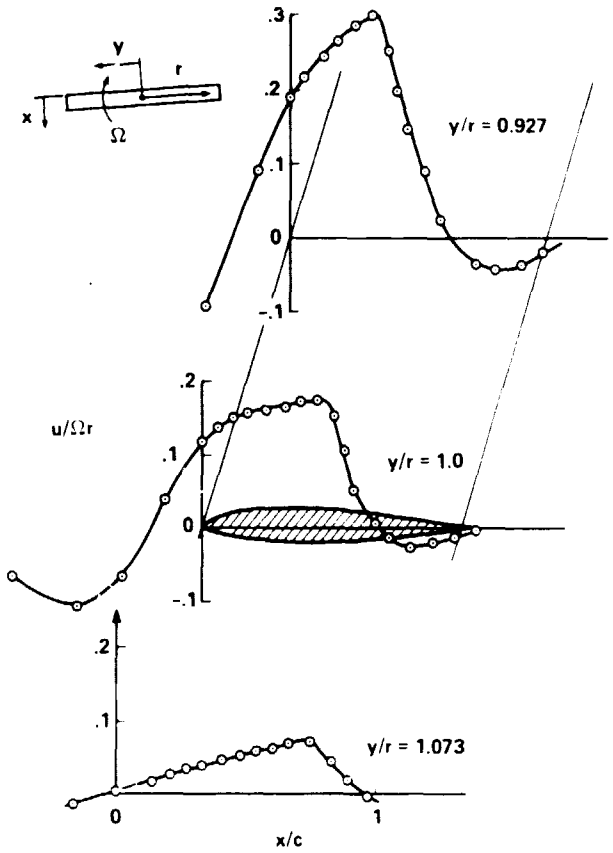

Fig. 22. Induced chordwise perturbation velocity profiles, Ames-Army anechoic chamber

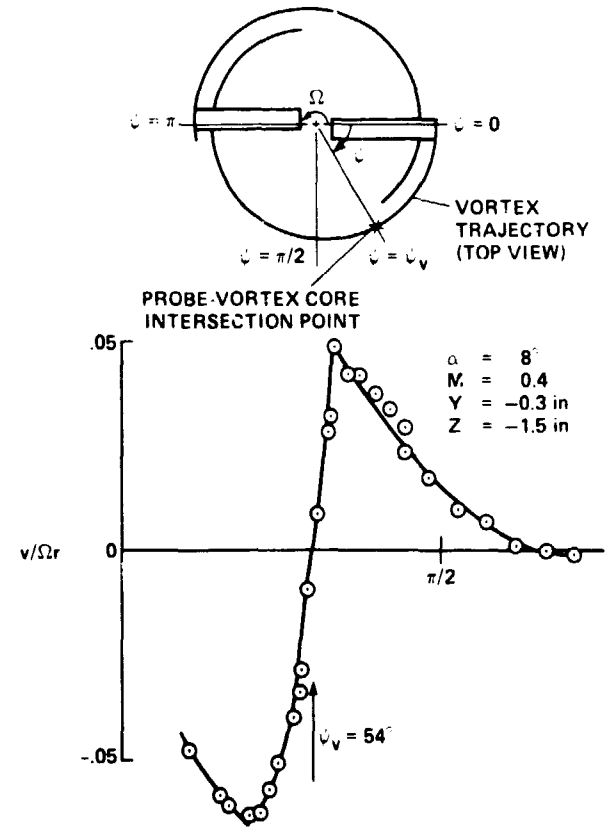

Fig. 23. Trailing vortex measurements, Ames-Army anechoic chamber.